Exact solution of a model of diffusion in an infinite chain or monolayer of cells coupled by gap junctions

S. V. Ramanan and P. R. Brink
Department of Physiology and Biophysics, Health Sciences Center, State University of New York, Stony Brook, New York 11794

ABSTRACT Analytic solutions are found for an infinite chain of cells coupled by gap junctions under two initial conditions: (*a*) One inner cell initially filled uniformly to a fixed concentration and (*b*) inner cell maintained indefinitely at constant concentration. The solution can be extended by the product method (Carslaw and Jaeger. 1959. Conduction of Heat in Solids. Oxford University Press.) to monolayers. We can also incorporate leakage through the plasma membrane by the product method. We demonstrate the utility of these results by fitting diffusion data from the septate axon of earthworm and by plots of theoretical profiles from monolayers of cells. Use of these analytic solutions enables one to overcome the limitations of methods thht lump the effects of cytoplasmic diffusion and junctional permeability into an effective diffusion coefficient.

INTRODUCTION

The synthesis of specific molecules over brief time intervals by a cell or group of cells and the subsequent diffusion of these molecules through a tissue is thought to be the basis for phenomena such as morphogenesis. These molecules or morphogens are believed to trigger cellular processes which then lead, for example, to differentiation. In practice, diagnosing the nature of the pathway(s) within and between cells in a tissue is achieved by modeling and subsequent analysis of the movement of exogenous probes such as fluorescent molecules where the mobility of the probe is assumed to be governed by passive diffusion. Adherence to passive diffusive behavior (1) appears not to be dependent on the cell system or tissue but is highly probe dependent, as illustrated by the contrast between the decline of Lucifer Yellow's mobility over time as against the constancy of mobility for molecules like carboxyfluorescein (2, 3).

A number of approaches have been utilized to demonstrate intercellular transfer of solutes via gap junctions (4, 5). A particularly useful approach has been analysis of probe transfer between isolated cell pairs linked by gap junctions (6, 7). In this case the cytoplasmic mobility can be ignored because of small cell size. Diffusion within monolayers of cells (8, 9) or anisotropic bundles of cells (10–12) is characterized by an effective diffusion coefficient (D_e). The D_e for a probe within a tissue is determined by both its mobility within the cytoplasm and its permeability through the gap junctional membrane. Endogenously and exogenously induced changes in the effective diffusion coefficient can thus be attributed to either the cytoplasmic coefficient or junctional membrane patency. The relation between the cytoplasmic diffusion coefficient (D), junctional membrane permeability (P^j), and the effective or apparent diffusion coefficient is given by

$$\frac{1}{D_e} = \frac{1}{D} + \frac{1}{2aP^j} \tag{1}$$

(10; Eq. 1 in Appendix by Hodgkin), where $2a$ equals the distance between successive junctional membranes. The validity of this relationship requires that $2a$ (typically microns) is much smaller than the distribution of the tracer (typically millimeters) within the tissue. This allows the tissue to be treated as a continuum. The above equation is clearly inappropriate when cell diameter or length is comparable to the length of distribution of the probe. In the case of a monolayer of cells, the distribution would presumably have to be at least an order of magnitude greater than cell diameter to justify decomposition of D_e into its component parts, D and P^j by the relation (1). Independent determination of D will not enable such a decomposition as long as radial distribution and cell length are comparable. This necessitates the development of analytic calculations which allow for determination of both the cytoplasmic diffusion coefficient and the gap junctional membrane permeability as independent parameters.

Programs to generate theoretical profiles can be obtained from the authors.

In cell systems with simple geometries that approximate a small number of cells linked in series by gap junctions, unique analytical mathematical solutions are possible. In this circumstance, the diffusion path is essentially one dimensional. Under such constraints, we can independently determine the cytoplasmic diffusion coefficient of a molecule and the gap junctional membrane permeability (3).

In this study, we present analytical solutions of diffusion in systems with an infinite number of cells. The system can be one dimensional (a chain) or two dimensional (monolayer). We consider two initial conditions, one where a cell is initially filled and the probe diffuses into other cells thereafter, and the other where one cell is maintained indefinitely at a fixed concentration. We can also incorporate leakage of the probe through the plasma membrane. In all cases, the parameters D and P^j are considered autonomous and can be determined independently from experimental data. We demonstrate the utility of the theoretical approach by fitting experimental data from a linear arrangement of cells; we further plot theoretical profiles for monolayers.

THEORY

We consider the model of an infinite number of identical cells linked in series with junctional membranes at the interfaces. The initial condition consists of an interior cell filled to a uniform concentration C^0 with a probe. The probe is assumed to permeate through the membranes and diffuse passively in the interior of the cells. We consider two cases: (*a*) the inner cell is initially filled with the probe and left undisturbed thereafter. (*b*) The concentration of probe in the inner cell is maintained uniformly and continuously.

INNER CELL INITIALLY FILLED

The width of each cell is taken to be $2a$. The origin of the axes is defined to be at the midpoint of the cell that is initially filled with the probe. Due to the symmetry of the problem around the point $x = 0$, there is no loss of generality in considering only the region $x \geq 0$. The concentration in the center cell is denoted by C_1, and the concentration in the ith cell outward is labeled C_i. The junctional membrane permeability and the cytosolic diffusion coefficient are denoted by P^j and D, respectively, and h stands for the ratio P^j/D. The following set of differential equations then develop:

(*a*) Diffusion

$$D\frac{\partial^2 C_1}{\partial x^2} = \frac{\partial C_1}{\partial t} \qquad 0 < x < a$$

$$D\frac{\partial^2 C_i}{\partial x^2} = \frac{\partial C_i}{\partial t} \qquad (2i-3)\,a < x < (2i-1)a \quad i = 2, 3, \ldots$$

(*b*) Transport

$$D\frac{\partial C_i}{\partial x} = D\frac{\partial C_{i+1}}{\partial x} = P^j\,(C_{i+1} - C_i)$$

$$x = (2i-1)a \quad i = 1, 2, \ldots$$

(*c*) Boundaries

$$C_1 = C^0 \quad 0 < x < a \quad t = 0.$$

$$C_i = 0 \qquad i > 1 \qquad t = 0.$$

$$\lim_{i\to\infty} C_i(t) = 0.$$

(*d*) Symmetry

$$\frac{\partial C_1}{\partial x}(0, t) = 0.$$

Define the Laplace transform of C_i by

$$\overline{C}_i(x, p) = \int_0^\infty e^{-pt} C_i(x, t)\, dt.$$

The transformed equations are

$$D\frac{d^2\overline{C}_1}{dx^2} = p\overline{C}_1 - C^0 \quad 0 < x < a; \ \ldots;$$

$$D\frac{d^2\overline{C}_i}{dx^2} = p\overline{C}_i \quad (2i-3)\,a < x < (2i-1)\,a \qquad (2)$$

$$D\frac{d\overline{C}_i}{dx} = D\frac{d\overline{C}_{i+1}}{dx} = P^j(\overline{C}_{i+1} - \overline{C}_i) \quad x = (2i-1)\,a \qquad (3)$$

$$\operatorname{Lt}_{j\to\infty} \overline{C}_j(x, p) = 0 \qquad (4)$$

$$\frac{d\overline{C}_1}{dx}(0, p) = 0. \qquad (5)$$

Define $q^2 = p/D$. The form of Eqs. 2 then prompts the following

$$\overline{C}_1(x, p) = A_1(p)e^{qx} + B_1 e^{-qx} + \frac{C^0}{Dq^2}$$

$$\overline{C}_i(x, p) = A_i(p)e^{qx} + B_i e^{-qx}.$$

The C_i's now satisfy Eqs. 2. Eq. 4 yields $\operatorname{Lim}_{i\to\infty} A_i(p) = 0$ while Eq. 5 implies the condition $A_1 = B_1$.

Inserting into Eqs. 3 and casting into matrix form gives

$$D_2 = T_1 D_1 + E_1; \qquad D_{i+1} = T_i D_i \quad i > 1,$$

where

$$D_i = \begin{bmatrix} A_i(p) \\ B_i(p) \end{bmatrix}; \quad E_1 = \frac{C^0}{2Dq^2}\begin{bmatrix} e^{-qa} \\ e^{qa} \end{bmatrix}$$

and

$$T_i = \begin{bmatrix} 1 + \dfrac{q}{2h} & -\dfrac{q}{2h} e^{-2qa(2i-1)} \\ \dfrac{q}{2h} e^{2qa(2i-1)} & 1 - \dfrac{q}{2h} \end{bmatrix}.$$

It is impossible to diagonalize all of the T_i's simultaneously. However, we demonstrate in Appendix 1 that we can find a quasi-diagonalization of the form $T_i = P_i \overline{T} \cdot P_{i-1}^{-1}$ for all i, where $\overline{T}$ is a diagonal matrix independent of i. The relevant results from the appendix are

$$P_i = \begin{bmatrix} e^{-2iqa} & e^{-2iqa} \\ A_+ e^{2iqa} & A_- e^{2iqa} \end{bmatrix}; \quad \overline{T} = \begin{bmatrix} g & 0 \\ 0 & g' \end{bmatrix}.$$

$A_\pm$ are the roots of the equation

$$A^2 - 2A\left[\frac{2h}{q}\sinh(2qa) + \cosh(2qa)\right] + 1 = 0.$$

Note $A_+ A_- = 1$. Explicitly, A_+ is given by

$$A_+ = \cos h(2qa) + \frac{2h}{q}\sin h(2qa) + \sqrt{\sin h(2qa)\left\{\sin h(2qa)\left(1 + \frac{4h^2}{q^2}\right) + \frac{4h}{q}\cos h(2qa)\right\}}.$$

The function g is specified by $g = e^{2qa}\{1 + (q/2h) - (q/2h)\, e^{-2qa} A_+\}$ and $g' = 1/g$.
The quasi-diagonalization is not possible if $A_+ = A_-$. Ignoring this for now, we find

$$D_{i+1} = T_i T_{i-1} \ldots T_2 T_1 D_1 + T_i T_{i-1} \ldots T_2 E_1 = P_i \overline{T}^i P_0^{-1} D_1 + P_i \overline{T}^{i-1} P_1^{-1} E_1.$$

Substituting for the matrices P and T, we find upon inversion

$$D_1 + E_1 = \frac{1}{(A_- - A_+)} \times \begin{bmatrix} (g'^i A_- - g^i A_+) e^{2iqa} & (g^i - g'^i) e^{-iqa} \\ (g'^i - g^i) A_+ A_- e^{2iqa} & (A_- g^i - A_+ g'^i) e^{-2iqa} \end{bmatrix} D_{i+1}.$$

Now from Eq. 4, we have

$$\lim_{i\to\infty} D_i = \begin{bmatrix} 0 \\ B_\infty \end{bmatrix}.$$

This enables us to solve for A_1 yielding

$$A_1 = \lim_{i\to\infty} \frac{C^0}{Dq^2} \frac{g^i(e^{qa} - A_- e^{-qa}) + g'^i(A_+ e^{-qa} - e^{qa})}{g^i(A_- - 1) + g'^i(1 - A_+)}.$$

In Appendix 2, we demonstrate that the denominator of the expression for A_1 has no roots in the complex q-plane except for the trivial one at $q = 0$. However, there are a number of branch points. One is at $q = 0$ and is due to the presence of $q = \sqrt{p/D}$. Other branch points occur at an infinite number of values of q where $A_+ = A_-$ on the negative p-axis at $p = -D\theta_r^2$. The contour for determining the Laplace inverse is thus chosen to avoid the pole at $p = 0$ and the branch cuts $(\theta_{2r}, \theta_{2r+1})$ for $r = 0, 1, 2, \ldots$.

In any branch cut $(\theta_{2r}, \theta_{2r+1})$ we have $A_+ > A_-$ and $g < g'$. In this case, on taking the limit in the expression for A_1 above, we find

$$A_1 = \frac{C^0}{Dq^2} \frac{A_+ e^{-qa} - e^{qa}}{1 - A_+}.$$

Thus

$$\overline{C}_1(x, p) = \frac{C^0}{Dq^2}\left\{1 + \cosh(qx) \frac{A_+ e^{-qa} - e^{qa}}{1 - A_+}\right\}.$$

Contour integration then gives

$$C_1(x, t) = -C^0 + \frac{2C^0}{\pi} \sum_{r=0}^{\infty} \int_{\theta_{2r}}^{\theta_{2r+1}} \cdot \frac{du}{u} e^{-Du^2 t} \cos(ux) \sin(ua) \frac{A_+(iu) + 1}{A_+(iu) - 1}.$$

From the equation $D_{i+1} = T_i D_i$, we can now calculate $\overline{C}_i(x, p)$ and invert to obtain $C_i(x, t)$. We only present the results:

$$C_i(x, t) = \frac{2C^0}{\pi} \sum_{r=0}^{\infty} \int_{\theta_{2r}}^{\theta_{2r+1}} \frac{du}{u} e^{-Du^2 t} \cdot \left\{\cos ux - G_i\left(ux, ua, \frac{u}{2h}\right)\right\} \sin ua \frac{A_+(iu) + 1}{A_+(iu) - 1}. \quad (6)$$

We give the explicit form of the first few $G_i = G_i(d, e, f)$:

$$G_2 = f\{\sin d - \sin(d - 2e)\}$$

$$G_3 = f\{2\sin d - \sin(d - 2e) - \sin(d - 6e)\} - f^2\{-\cos d + \cos(d - 2e) + \cos(d - 4e) - \cos(d - 6e)\}$$

$$G_4 = f\{3\sin d - \sin(d-2e) - \sin(d-6e) - \sin(d-10e)\} - f^2\{-3\cos d + 2\cos(d-2e) + 2\cos(d-4e) + \cos(d-8e) - 2\cos(d-10e)\} - f^3\{2\sin d - 2\sin(d-2e) - 4\sin(d-4e) + 4\sin(d-6e) + 2\sin(d-8e) - 2\sin(d-10e)\}.$$

INNER CELL CONTINUOUSLY FILLED

We use the same notation as in the previous section. The differential equations are

(*a*) Diffusion

$$D\frac{\partial^2 C_i}{\partial x^2} = \frac{\partial C_i}{\partial t} \qquad (2i-3)a < x < (2i-1)a \quad i = 2, 3, \ldots$$

(*b*) Transport

$$D\frac{\partial C_2}{\partial x} = P^j(C_2 - C^0) \qquad x = a$$

$$D\frac{\partial C_i}{\partial x} = D\frac{\partial C_{i+1}}{\partial x} = P^j(C_{i+1} - C_i) \quad x = (2i-1)a \quad i = 2, 3, \ldots$$

(*c*) Boundary

$$C_i = 0 \quad i > 1 \quad t = 0$$

$$\operatorname*{Lt}_{i\to\infty} C_i(t) = 0.$$

Applying the Laplace transform and proceeding in much the same way as in the previous section we find

$$A_2 = -\operatorname*{Lt}_{i\to\infty}\frac{hC^0}{Dq^2}\times\frac{(g^{i-1} - g'^{i-1})e^{-2qa}}{g^{i-1}\{(q-h)e^{-qa} - (q+h)e^{qa}A_-\} - g'^{i-1}\{(q-h)e^{-qa} - (q+h)e^{qa}A_+\}}.$$

The contour for finding the inverse transform is the same as in the previous section. Proceeding to the limit by using $A_+ > A_-$, $g < g'$ we obtain

$$A_2 = -\frac{hC^0}{Dq^2}\frac{e^{-2qa}}{(q-h)e^{-qa} - (q+h)e^{qa}A_+}$$

and similarly

$$B_2 = -\frac{2hC^0}{Dq^2}\frac{e^{2qa}A_+}{(q-h)e^{-qa} - (q+h)e^{qa}A_+}.$$

Contour integration then yields

$$C_2(x,t) = \frac{2h^2C^0}{\pi}\sum_{r=0}^{\infty}\int_{\theta_{2r}}^{\theta_{2r+1}}\frac{du}{u} \cdot e^{-Du^2t}Z\left\{\sin(ux-ua) + H_2\left(ux, ua, \frac{u}{2h}\right)\right\},$$

where H_2 is specified below and

$$Z = \frac{[1 - A_+(iu)]^2}{(h^2+u^2)\{1 + A_+^2(iu) + 2\{(h^2-u^2)\cos 2ua - 4uh\sin 2ua\}A_+(iu)}.$$

Again we can use $D_{i+1} = T_iD_i$ to calculate $C_i(x, t)$ for $i > 2$. The results are

$$C_i(x,t) = C^0 - \frac{2h^2C^0}{\pi}\sum_{r=0}^{\infty}\int_{\theta_{2r}}^{\theta_{2r+1}} \cdot\frac{du}{u}e^{-Du^2t}Z\left\{\sin(ux-ua) + H_i\left(ux, ua, \frac{u}{2h}\right)\right\}. \quad (7)$$

The first few $H_i = H_i(d, e, f)$ are as below:

$$H_2 = 2f\cos(d-e)$$

$$H_3 = f\{3\cos(d-e) + \cos(d-5e)\} - f^2\{\sin(d-e) - \sin(d-5e)\}$$

$$H_4 = f\{4\cos(d-e) + \cos(d-5e) + \cos(d-9e)\} + f^2\{-5\sin(d-e) + 2\sin(d-5e) + 3\sin(d-9e)\} + 2f^3\{-\cos(d-e) + 2\cos(d-5e) - \cos(d-9e)\}.$$

TRANSVERSE DIFFUSION

We consider the case of a circular cell of radius R, initially filled to a concentration C^0, interfacing to a bath with an effectively infinite diffusion coefficient through a membrane of permeability P^m. The differential equations are

$$\frac{1}{r}D\frac{\partial}{\partial r}\left[r\frac{\partial C}{\partial r}\right] = \frac{\partial C}{\partial t} \qquad r < R$$

$$D\frac{\partial C}{\partial r} = P^mC \qquad r = R.$$

The average concentration in the disk is then given by

$$C = \frac{4C^0}{R^2}\sum_{n=0}^{\infty}e^{-a_n^2tD}\frac{h_m^2}{a_n^2(h_m^2 + a_n^2)}, \quad (8)$$

where $h_m = P^m/D$. The a_n's are the roots of the equation (1, p. 493).

$$a_nJ_1(a_nR) - h_mJ_0(a_nR) = 0.$$

and J_0 and J_1 are the Bessel functions conventionally defined (1, Appendix 3).

PRODUCT SOLUTIONS

As explained in Carslaw and Jaeger (1, p. 33), we can find solutions to problems of diffusion in two- or three-dimensional cubes with or without transverse leakage by taking appropriate products of the solutions presented in the above sections and in reference 3. Such product solutions are useful, for example, in the modeling of monolayer geometries relevant to experimental setups. Thus, for diffusion in a monolayer of square cells in the xy plane, with leak in the z-axis, the concentration is given by

$$C(x, y, z, t) = C(x, t, \text{Eq. 6}) \times C(y, t, \text{Eq. 6}) \times C(z, t, \text{reference 3.})$$

Here the central cell is uniformly filled with probe at $t = 0$ with passive diffusion prevailing thereafter.

METHODS

Experimental methods are the same as those outlined in reference 3. The cells are the neurons which comprise the septate axon system of the earthworm. The neurons have axons which are ~1 mm in length and 80–100 μm in diam. The cylindrical axons lie end-to-end and form gap junctions at the sites of close contact (14, 15). The apposition of two adjacent axons is called a septum. A single axon was injected with probe as described in reference 3. The nerve cord in which the individual axons lie was perfused with saline before injection. The saline solution contained 130 mM NaCl, 0.5 mM KCl, 1 mM $MgCl_2$, 1 mM $CaCl_2$, and 10 mM Hepes, pH = 7.25. After injection the preparation was cooled 5°C/min to a temperature of 5–6°C. Of the two experimental profiles shown, the solvent was deuterium oxide in one case (Fig. 1) and water in the other (Fig. 2). The diffusion probe used was dichlorofluorescein.

COMPUTATION

Numerical evaluation of the concentration integral can be split into two parts: (*a*) The branch points θ, which are the endpoints for the evaluation of the integrals in the infinite series for the concentration, are the zeros of the expression

$$\cos(2\theta a) + \frac{2h}{\theta}\sin(2\theta a) = \pm 1.$$

The zeros θ_r are given by $r\pi/2a$. The odd zeros are bracketed by the even zones, and are thus easily determined by the Newton-Raphson method (13, p. 254). This computation has to be done only once for a given value of h, and the results can thereafter be used for calculation of the concentration at all distances and times.

(*b*) The actual evaluation of the integrals is done by the method of Burlisch and Stoer (13, p. 563). We have verified that ~50 branch points are sufficient to assure convergence to an accuracy of 10^{-4} for P in the range 10^{-2}–10^{-8}cm/s, D in the range 10^{-3}–10^{-9} cm^2/s, and cell width from 0.1 to 10^{-4} cm. Accuracy is monitored in all cases by checking against the known profiles at $t = 0$. The

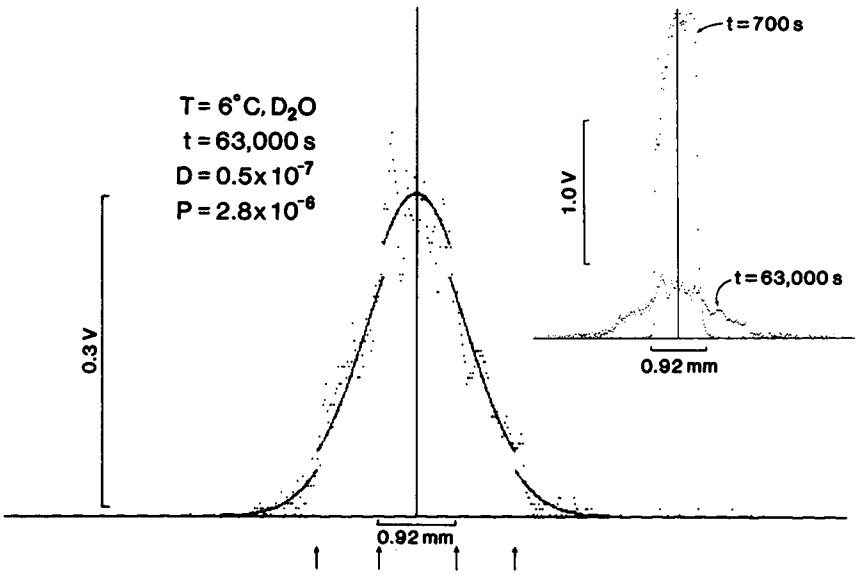

FIGURE 1 Dye concentration (digitized points) at 63,000 s from earthworm axons. The center cell was injected initially to a uniform concentration ($t = 700$ s profile in the inset) and diffusion was monitored. The solid line is the fit obtained as detailed in the text with diffusion coefficient and junctional permeability equal to 0.5×10^{-7} cm^2/s and 2.8×10^{-6} cm/s, respectively. The inset shows the profiles at ~0 and 63,000 s on the same scale to facilitate comparisons. The solvent used for the perfusate was deuterium oxide.

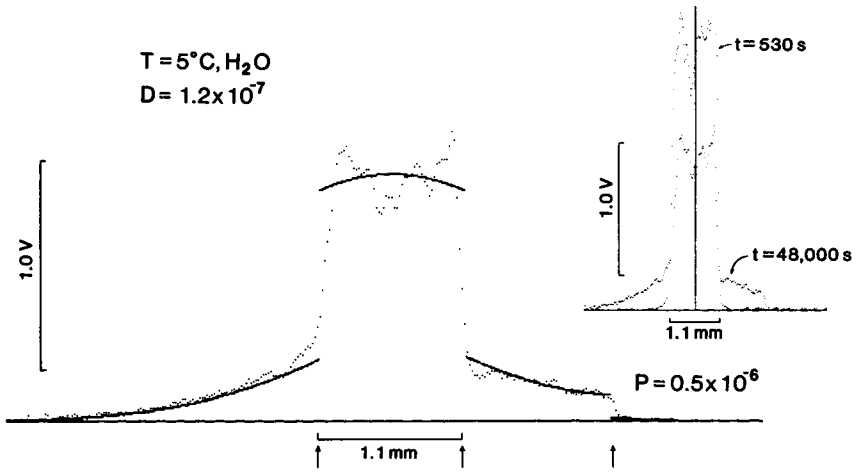

FIGURE 2 Profile of dye concentration (digitized points) at 48,000 s. As in Fig. 1, the inner cell was initially filled uniformly with dye and subsequent diffusion was passive. The inset shows the profiles at 530 s and 48,000 s on the same scale. Because of the assymmetry in the cells to the left and right of the injected cell, the fits to the two sides were computed differently. The right side was fitted by using Eq. 6 in the text; thus we have assumed a linear infinite chain of cells. The left side was predicted using the methods of Eq. 3; here *one* infinitely long cell is assumed to lie apposite to the injected cell. The parameters chosen for the two fits, however, are the same, namely $D = 1.2 \times 10^{-7}$ cm^2/s and $P^j = 0.5 \times 10^{-6}$ cm/s. The solvent used in the perfusate was water.

infinite series for the concentration converges very rapidly for all times, including $t = 0$. A typical time for evaluation of the concentration at a point, after the initial determination of branch points, is ~0.5 s in compiled BASIC on a 386 PC.

RESULTS

The diffusion of the fluorescent probe dichlorofluorescein within a linearly arranged group of neurons is shown in Fig. 1. The inset of Fig. 1 shows two scans: one is the initial diffusion profile 700 s after termination of injection while the second scan shows the distribution at 63,000 s. An enlargement of the scan at 63,000 s is shown in the rest of Fig. 1. The arrows indicate the septa, the regions of close apposition between two adjacent axons. This data set is fit to the theoretical profile generated by the cross-product (Eq. 6) × (Eq. 8). The cytoplasmic diffusion coefficient is 0.5×10^{-7} cm^2/s and the gap junctional membrane permeability is 2.8×10^{-6} cm/s. The preparation was perfused with a deuterium oxide saline.

Fig. 2 shows another diffusion profile from an experiment where there is no symmetry around the injected cell. In this case, the temperature was 5°C and the solvent was water. The insert of Fig. 2 shows the profiles at 530 and 48,000 s after injection while the main figure is an enlargement of the 48,000 s profile. Note that the cells to the right of the central cell are of approximately the same length while to the left no septa can be discerned. The fit to the right of the midpoint of the central cell is accordingly made as in the previous figure while that to the left is generated by the analysis of reference 3. The cytoplasmic diffusion coefficient was 1.2×10^{-7} cm^{-2}/s and the junctional permeability was 0.5×10^{-6} cm/s; note that both sides of the diffusion profile are fit with the same parameters. The fact that the fit is reasonably good on both sides thus suggests that the analytic solution is fairly robust with regard to assymmetries in the experimental setup.

The diffusion data fit in Figs. 1 and 2 is for rather large linear cells. As outlined in the theory section, the analytical solutions can also be used for monolayers. In Figs. 3–5, we present theoretical concentration profiles for diffusion in a monolayer of small cubic cells with side length equal to 10^{-3} cm and the center cell is filled with dye at $t = 0$. There is a leak to the external bath across the two faces of each cell which face the bath, the transverse permeability being fixed at 1×10^{-9} cm/s. Fig. 3 shows the profiles at 10 s of four different cases where the diffusion coefficient D is fixed at 10^{-7} cm^2/s while the junctional permeability P^j is varied from 5×10^{-5} to 10^{-2} cm/s. It can be seen that there are distinct steps in the profile at the junctional interface until P^j is increased to 10^{-3} cm/s. The profiles inside the cells are fairly flat at the value of D we have assumed; thus the junctional steps would be discernible in experimental data if $P^j \approx < 10^{-4}$ cm/s i.e., when the dimensionless parameter (see Eq. 1) given by $2aP^j/D \approx < 1$.

Fig. 4. shows plots of the theoretical profiles for various cases where P^j is fixed at 10^{-4} cm/s while D is varied from

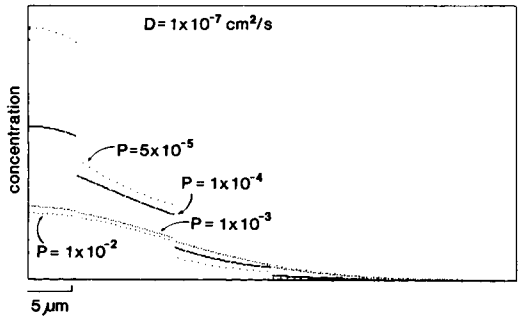

FIGURE 3 Concentration profiles at 10 s for a monolayer of square cells with side ($=2a$) and height of 10^{-3} cm. The center cell is initially injected uniformly with dye and passive diffusion takes place thereafter. There is a leak to the external bath across the top and bottom faces of each cell; the transverse permeability is 10^{-9} cm/s. The cytoplasmic diffusion coefficient D is fixed at 10^{-7} cm^2/s while the junctional permeability P^j is varied from 5×10^{-5} to 10^{-2} cm/s. Note the disappearance of steps at the cell interface as the junctional permeability is increased.

10^{-8} to 10^{-6} cm^2/s. The profiles inside the cells are fairly flat and there are steps at the junctional interface for all the D's shown. However, at $D = 1 \times 10^{-8}$ cm/s, it can be seen that the main changes in the profiles occur inside the cells and the drop in the interface is only a small fraction of the change inside in the cells. Alternatively, we can say that the curvature of the profile inside the cell is so large that it begins to approach the infinite value at the interface. Experimentally derived profiles contaminated by noise would smear the profile and render the detection of steps at the junctional interface impossible. The drop at the junction becomes important, however, when D is $>\approx 10^{-7}$ cm/s, i.e., when the dimensionless parameter $2aP^j/D \simeq <1$.

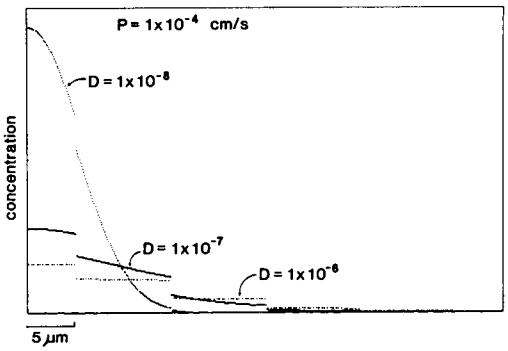

FIGURE 4 All the conditions are the same as in Fig. 3, except that P^j is fixed at 10^{-4} cm/s while D is varied from 10^{-8} to 10^{-6} cm^2/s. In the presence of photoelectric noise normally encountered in monitoring fluorescent intensity, discontinuities at the cell interface would not be visible when $D = 10^{-8}$ cm^2/s.

Fig. 5 shows three concentration profiles where the diffusion coefficient is fixed at 10^{-7} cm^2/s. The junctional permeability in the three panels are 10^{-3} cm/s, 10^{-4} cm/s, and 10^{-5} cm/s; all the other parameters are the same as in Figs. 3 and 4. The dimensionless parameter $2aP^j/D$ for the three panels is then 10, 1, and 0.1, respectively. It is seen from comparison of the profiles that the drops across the junction would be imperceivable in the first panel in the presence of noise; in the second panel the steps at the cell interfaces are visible until the time is ~40 s while the conditions of the third panel permit the junctional discontinuities to be discerned even at 40 s, the longest time at which we have plotted the profiles.

CONCLUSION

We have presented an analytic method which allows fitting of diffusion concentration profiles for arbitrary

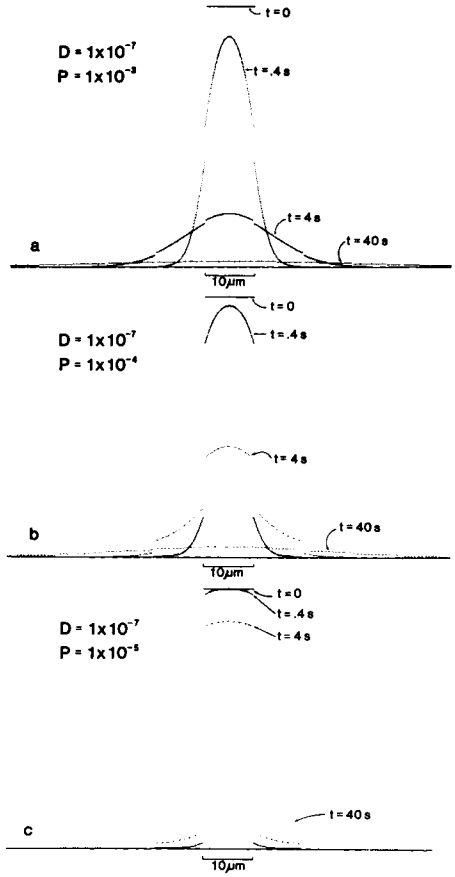

FIGURE 5 The dimensions of the cell monolayer and leak to the external bath are as in Figs. 3 and 4. D is fixed at 10^{-7} cm^2/s, while P^j in a, b, and c is 10^{-5}, 10^{-4}, and 10^{-3} cm/s, respectively. Each panel shows the concentration profiles at 0.4, 4, and 40 s.

times with two independent parameters: the cytoplasmic diffusion coefficient inside the cell and the permeability of the gap junctional membrane. This enables the effects of changes on these parameters by exogenous stimuli, for example, to be determined individually without recourse to the use of an effective diffusion coefficient. The determination of the cytoplasmic diffusion coefficient and gap junctional permeability via the methods presented here is still possible even when cell length is comparable to the length scale of the probe distribution. It may be noted that extraction of parameters P^j and D by iterative fitting of analytic solutions to the experimental profiles is a fairly rapid process numerically.

From Figs. 3–5, it can be noted that when the dimensional parameter $2aP^j/D \simeq >10$ for cells of linear dimension 10^{-3} cm, then steps at the junctional interface cannot be detected in the concentration profiles. From Eq. 1, we can estimate the contribution of the permeability to the effective diffusion coefficient in this case to be ~10%. Thus if no steps are seen in the profile, it would suggest that the cytoplasmic diffusion coefficient is a major contributor to the overall diffusion profile for large aggregates of cells of length 10^{-3} cm. The presence or absence of steps at the junctions in the data is thus a clear demarcator in the discrimination of the importance of the relative contributions of D and P^j to overall diffusion.

The solutions demonstrated here are pertinent to the evolution of the diffusion equations for a number of perfect grids, including square, cubic, and cylindrical. Experimental geometries are more complicated and often assymmetrical. It seems reasonable, however, that the method given above will be a good approximation when the tissue is homogeneous. The average of the concentration at a given radius from the center of the injected cell would presumably be an approximate invariant only weakly dependent on cell geometry, thus not critically dependent on whether the geometry is cubic or hexagonal, for instance. Fig. 2 is a good illustration of the matching of two different solutions to an assymmetric profile, where identical parameters are predicted by fits to both the sides.

APPENDIX 1

T_i is given by the expression

$$T_i = \begin{bmatrix} 1 + \frac{q}{2h} & -\frac{q}{2h} e^{-2qa(2i-1)} \\ \frac{q}{2h} e^{2qa(2i-1)} & 1 - \frac{q}{2h} \end{bmatrix}.$$

Note determinant $T_i = \|T_i\| = 1$. Let us examine if a decomposition of the type $T_i = P_i \overline{T}_i P_{i-1}^{-1}$ is possible for all i, where $\overline{T}_i$ is diagonal and P_i, $\overline{T}_i$ have the forms

$$P_i = \begin{bmatrix} x_i & x_i' \\ y_i & y_i' \end{bmatrix}; \quad \overline{T}_i = \begin{bmatrix} g_i & 0 \\ 0 & g_i' \end{bmatrix}$$

with $\|P_i\| \neq 0$. Denote $z_i = y_i/x_i$, $z_i' = y_i'/x_i'$. Then using $T_i P_{i-1} = P_i \overline{T}_i$ and eliminating g_i we find

$$z_i - z_{i-1} + \frac{q}{2h}(z_i + z_{i-1}) = \frac{q}{2h}\{e^{2(2i-1)qa} + e^{-2(2i-1)qa} z_i z_{i-1}\}.$$

The i dependence can be eliminated by the subsitution $z_i = A \exp \cdot (4iqa)$. A then satisfies

$$A^2 - 2A\left\{\frac{2h}{q}\sinh 2qa + \cosh 2qa\right\} + 1 = 0.$$

with roots $A_\pm$. We choose $z_i = A_+ \exp(4iqa)$ and $z_i' = A_- \exp(4iqa)$. With this choice, it is seen that $\|P_i\| = x_i x_i' \exp(4iqa)\{A_+ - A_-\}$. If we let $x_i = x_i' = \exp(-2iqa)$, we further have $\|P_i\| = A_+ - A_-$ which is independent of i. Also we find

$$\|\overline{T}_i\| = \|P_i \overline{T}_i P_{i-1}^{-1}\| = \|T_i\| = 1.$$

Substitution now yields

$$g_i = e^{2qa}\left\{1 + \frac{q}{2h} - \frac{q}{2h} e^{-2qa} A_+\right\} \equiv g$$

$$g_i' = e^{2qa}\left\{1 + \frac{q}{2h} - \frac{q}{2h} e^{-2qa} A_-\right\} \equiv g'.$$

Thus the matrix $\overline{T}_i$ itself is independent of i as claimed.

APPENDIX 2

Consider functions $U_1, U_2, U_3, \ldots$ defined by

$$U_1 = G_1(e^{-\beta x} + e^{-\beta x}) \qquad 0 < x < a$$

$$U_i = G_i e^{-\beta x} + H_i e^{-\beta x} \quad (2i-3)a < x < (2i-1)a$$

and

$$\begin{bmatrix} G_i \\ H_i \end{bmatrix} = T_{i-1}(\beta) \begin{bmatrix} G_{i-1} \\ H_{i-1} \end{bmatrix},$$

where T_i is as given in Appendix 1 with q replaced by β.

The U_i then satisfy the equations $d^2U_i/dx^2 = \beta^2 U_i$ in the interior of the domains of definition and the equations

$$\frac{dU_i}{dx} = \frac{dU_{i-1}}{dx} = h(U_{i-1} - U_i)$$

at the appropriate boundaries. Further, symmetry about the origin is maintained as $dU_1/dx = 0$ at $x = 0$.

Proceeding in the same way as in Appendix 1 we obtain

$$G_1 = \underset{i\to\infty}{Lt} \frac{B_i}{A_- - A_+}(g^i - g'^i) e^{-2iqa}$$

$$G_1 = \underset{i\to\infty}{Lt} \frac{B_i}{A_- - A_+}(A_- g^i - A_+ g'^i) e^{-2iqa}.$$

This is satisfied if β is a root of

$$g^i(A_- - 1) + g'^i(1 - A_+) = 0 \qquad (6)$$

in the limit $i \to \infty$.

Now let α be another root of Eq. 6 with V_i being the corresponding associated function. Using the differential equations satisfied by U_i, V_i we can show

$$(\beta^2 - \alpha^2)\left[\int_0^a dx\, U_1 V_1 + \int_a^{3a} dx U_2 V_2 + \cdots\right] = 0.$$

If α and β are complex conjugates then we have $\beta^2 - \alpha^2 \neq 0$; but because U_i, V_i are then complex conjugates the term in square brackets is positive and we have a contradiction.

For real β we can show $A_+ > 1 > A_-$ and hence $|g| > 1 > |g'|$. In the limit $i \to \infty$, this implies that Eq. 6 has no solution for real β. Thus any roots of Eq. 6 exist only for imaginary β. If we disregard the points where $g = g'$, we can show, as for real β, that $g' > 1 > g$ or $g > 1 > g'$. In either case, for $i \to \infty$, we have no root for Eq. 6. Thus Eq. 6 is zero only at the points where $g = g'$. But this implies $A_+ = A_-$, so that these points are actually branch points.

The authors would like to thank Dr. R. T. Mathias and Dr. K. Manivannan for invaluable discussions and insight.

This work was supported by National Institutes of Health grant HL 31299.

Received for publication 22 August 1989 and in final form 8 March 1990.

REFERENCES

1. Carslaw, H. S., and J. C. Jaeger. 1959. Conduction of Heat in Solids. 2nd ed. Oxford University Press, Oxford. 505.
2. Stewart, W. 1978. Functional connection between cells as revealed by dye coupling with a highly fluorescent naphthalimide tracer. *Cell.* 14:141–159.
3. Brink, P. R., and S. V. Ramanan. 1985. A model for the diffusion of fluorescent probes in the septate giant axon of earthworm: axoplasmic diffusion and junctional membrane permeability. *Biophys. J.* 48:299–309.
4. Loewenstein, W. R. 1981. Junctional intercellular communication: the cell-to-cell membrane channel. *Physiol. Rev.* 61:829–913.
5. Jaslove, S. W., and P. R. Brink. 1987. Electrotonic coupling in the nervous system. *In* Cell-to-Cell Communication. W. C. DeMello, editor. Plenum Publishing Corp., New York. 103–147.
6. Atkinson, M. M., and J. D. Sheridan. 1985. Reduced junctional permeability in cells transformed by different viral oncogenes. *In* Gap Junctions. M. V. L. Bennett and D. C. Spray, editors. Cold Spring Harbor Laboratory, Cold Spring, New York. 205–213.
7. Biegon, R. P., M. M. Atkinson, T. F. Liu, E. Y. Kam, and J. D. Sheridan. 1987. Permeance of novikoff hepatoma gap junctions: quantitative video analysis of dye transfer. *J. Membr. Biol.* 96:225–233.
8. Safranyos, R. G. A., and S. Caveney. 1985. Rates of diffusion of fluorescent molecules via cell-to-cell membrane channels in a developing tissue. *J. Cell Biol.* 100:736–747.
9. Rae, J. L., A. W. Lewno, K. Cooper, and P. Gates. 1989. Dye and electrical coupling between cells of the rabbit corneal endothelium. *Curr. Eye Res.* 8:859–869.
10. Weidmann, S. 1966. The diffusion of radiopotassium across intercalated discs of mammalian cardiac muscle. *J. Physiol.* 187:323–342.
11. Weingart, R. 1974. The permeability to tetraethylammonium ions of the surface membrane and the intercalated disks of sheep and calf myocardium. *J. Physiol.* 240:741–762.
12. Cole, W. C., R. E. Garfield, and J. S. Kirkaldy. 1985. Gap junctions and direct intercellular communications between rat uterine smooth muscle cells. *Am. J. Physiol.* 249:C20–C31.
13. Press, W. H., B. P. Flannery, S. A. Teukolsky, and W. T. Vetterling. 1988. Numerical Recipes. Cambridge University Press, Cambridge, MA. 818 pp.
14. Brink, P. R., and M. M. Dewey. 1978. Nexal membrane permeability to anions. *J. Gen. Physiol.* 72:69–78.
15. Kensler, R. W., P. R. Brink, and M. M. Dewey. 1979. The septum of the lateral axon of the earthworm: a thin section and freeze fracture study. *J. Neurocytol.* 8:565–590.